Computers in Biology and Medicine 108 (2019) 332–344

Contents lists available at ScienceDirect

Computers in Biology and Medicine

journal homepage: www.elsevier.com/locate/compbiomed

Predictive modeling of drug effects on electrocardiograms

T. Peng[a,*], M.L. Trew[b], A. Malik[a]

[a] Department of Electrical and Computer Engineering, University of Auckland, 1010, New Zealand
[b] Auckland Bioengineering Institute, University of Auckland, Auckland, 1010, New Zealand

ARTICLE INFO

Keywords:
Electrocardiogram modeling
Morphological modeling
Signal decomposition
Morphological prediction
Drug effects on ECG

ABSTRACT

Whole electrocardiogram (ECG) waveform analysis is a technique for evaluating aggregate arrhythmic risks of drugs. In this paper, we propose methods for exploring changes to ECG morphology due to drug effects using Gaussian model parameters, and predict patient specific post-drug ECG based on pre-drug ECG. We evaluate the proposed methods using clinical ECG recordings from subjects under the effect of anti-arrhythmic drugs Dofetilide, Quinidine, Ranolazine, and Verapamil, from the ECGRVDQ database on PhysioNet. Paired-sample *t*-test p-values (>0.05) suggest the proposed method can achieve similar results when compared to expert annotated J to T_{peak} and T_{peak} to T_{end} intervals for all four drug states. We employed a leave-one-out cross validation strategy to train the prediction model and produce the results. Mean Pearson correlations between all predicted and recorded post-drug waveform morphologies for all drug states across both the vector magnitude lead and Lead II is 0.94 ± 0.05, with p-values <0.01 for all predictions; indicating significant predictions. Parameters from ECG models with Gaussian basis can be used to calculate clinically useful information and to capture or predict changes in cardiac signals due to drug effects.

1. Introduction

The electrocardiogram (ECG) is an important non-invasively recorded electrophysiological signal which is commonly used by clinicians to diagnose and monitor adverse heart conditions. To assess the aggregate arrhythmic risk for new drugs, a consortium of drug regulators (U.S. Food and Drug Administration, European Medicines Agency, Health Canada, Japan Pharmaceutical and Medical Devices Agency) and researchers have proposed the Comprehensive in vitro Proarrhythmia Assay, which includes ECG analysis as an integrated component alongside Phase 1 studies [1]. Such ECG analysis is often carried out under computer-aided expert attention and is limited to timing interval comparisons [2,3].

Parametric models of ECG signals have been proposed to effectively represent the complete ECG waveform morphology using basis functions, such as orthonormal exponentials [4], spline [5], and Gaussian [6] functions. In general, the basis function representations of ECGs can be expressed as Eq (1) [4], where $f(t)$ is a time-series of the recorded ECG, $\phi_i(t)$ is the i-th basis function component, c_i is the coefficient or parameter of the i-th basis function, N is the number of basis functions used, and $\varepsilon(t)$ is the time domain error between the basis representation and the clinically recorded ECG. In essence, given two ECG recordings from different cardiac states (normal, disease or drug) represented with the same basis function set ϕ, then the difference in morphology can be encoded as changes in the coefficients or parameter values c_i.

$$f(t) = \sum_{i=1}^{N} c_i \phi_i(t) + \varepsilon(t) \tag{1}$$

Model parameter values of recorded ECGs are useful for delineation of morphological features [7] and classification of disease states [8]. More recently, automated parameter identification for such models through bound constrained global optimization has been shown to be effective at capturing ECG in multiple disease states [9]. As an alternative ECG analysis method, such models offer feature extraction for representing and comparing changes in whole ECG waveform morphology in a reduced basis function parameter space.

In Ref. [10], the authors explored the efficacy of a variety of parametric ECG models with different basis functions and found that those with a Gaussian basis, such as [6,9], offered parameters with physiological interpretation relative to the standard P, Q, R, S, and T complexes of the ECG. This suggests that the parameters encode clinically useful timing and morphological information. Furthermore, the Gaussian basis set achieved the best signal compression error at low numbers of model basis functions.

Related Gaussian basis models, using Gaussian mesa functions [11], have been used to capture and analyze the change in repolarization

* Corresponding author. Department of Electrical and Computer Engineering, University of Auckland, 1010, Auckland, New Zealand.
E-mail address: tpen280@aucklanduni.ac.nz (T. Peng).

https://doi.org/10.1016/j.compbiomed.2019.03.027
Received 19 November 2018; Received in revised form 27 March 2019; Accepted 28 March 2019
0010-4825/

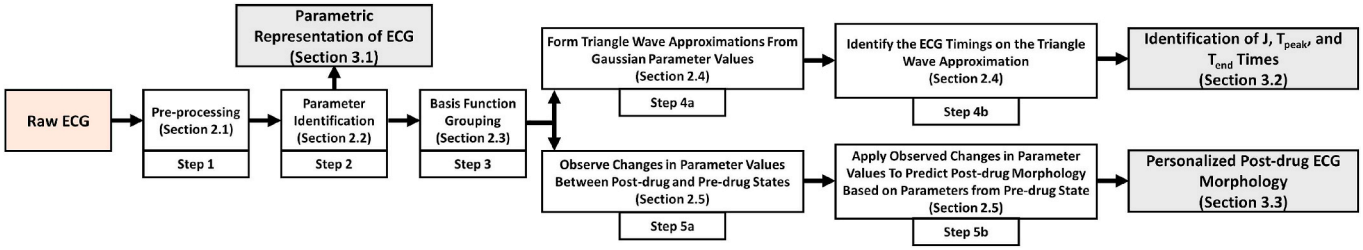

Fig. 1. Summary of methodology. Each step indicates the relevant section where it is described. The grey boxes are results and the orange box is the input clinical recordings.

$$w_i(t) = amp_i \cdot \exp\left[-\left(\frac{t - shift_i}{width_i}\right)^2\right] \tag{2}$$

$$g(t, \vec{x}) = \sum_{i=1}^{N} w_i(t) + b_s \tag{3}$$

morphology of ECGs due to drug effects [12]. However, to the best of our knowledge, the ability of Gaussian model parameters to predict whole waveform morphologies due to drug effects is unexplored. In this paper, we extend the model parameterization framework outlined in Ref. [9] to: ① quantify the aggregate changes due to drug effects for clinically recorded ECGs from the PhysioNet ECGRVDQ database [3,13] and ② predict post-drug ECG waveform morphologies using the reduced model parameter space. We validate the proposed prediction framework using a leave-one-out cross validation strategy, where recordings from all-but-one of the subjects is the training set, and the recordings from the remaining subject is the testing set. This process is repeated such that each subject is the testing set exactly once. The proposed method can predict changes to patient ECGs, which have high correlation with those found in the training set.

2. Methods

The overall methodology used in this paper is summarized in Fig. 1. The clinical ECG recordings from the ECGRVDQ database on PhysioNet [3,13] are preprocessed into individual drug datasets and Gaussian basis function parameters are identified through global optimization. Overlapping basis function sets, which represent the same ECG complexes are identified. Finally, these basis function sets are used to identify J to T_{peak} intervals, T_{peak} to T_{end} intervals, and predict patient specific post-medication ECGs.

2.1. Data preprocessing (Step 1)

Median ECG recordings, calculated with sample-by-sample synchronization of the QRS complex, were obtained from the ECGRVDQ database at PhysioNet [3,13]. The database contains ECG recordings from healthy subjects administered antiarrhythmic drugs in a randomized double-blind, 5-period crossover clinical trial conducted over 24-h periods for comparing the effects of the drugs. Pharmacokinetic measurements and expert annotated ECG timing intervals are also provided for each ECG recording. For the purposes of validating the framework proposed in this paper, the first 850 samples of vector magnitude lead (VM) and Lead II (LII) recordings under the influence of four drugs, Dofetilide (*subject count* 22), Quinidine (*subject count* 19), Ranolazine (*subject count* 20), and Verapamil (*subject count* 19), were processed into pre-drug and post-drug datasets in MATLAB®. The pre-drug state was the median recording made before administering the drug. The post-drug state median ECG recordings were taken from the first time the pharmacokinetic test showed 2000–2500 pg/mL for Dofetilide, 1000–1500 ng/mL for Quinidine, 1000–1500 ng/mL for Ranolazine, and 70–500 ng/mL for Verapamil. Paired recordings from subjects with both pre-drug and post-drug median recordings were extracted. The specific identification numbers for each ECG recording can be found in the Supplementary Materials.

2.2. ECG model and parameter identification (Step 2)

The ECG model used in this paper is inspired by the popular ECGSYN [6] parametric model with a Gaussian basis. Our model is a modified waveform morphology-only implementation from Ref. [9] with a varying number of Gaussian basis functions. The individual basis functions are mathematically described as Eq (2), and the full ECG waveform morphology can be produced through Eq (3). Here, $w_i(t)$ is the i-th basis component of the model. Each basis component is described by amp_i, $width_i$ and $shift_i$, which parametrizes the amplitude, component width, and peak timing from the start of the median clinical waveform recording, respectively. The final ECG waveform $g(t, \vec{x})$ can be found using Eq (3) where $\vec{x}$ is the vector of *amp*, *width*, and *shift* for all N basis components and b_s is a baseline value intended to model isoelectric shift.

The recording specific parameter identification problem is framed as a bound constrained global optimization problem and solved using Particle Swarm Optimization (PSO), similar to methods described in Ref. [9]. The minimization problem can be summarized as Eq (4), where RD is the root mean squared difference (defined in Eq (5)), $g(t, \vec{x})$ is the Gaussian model time-domain signal and ϕ_r is the clinically recorded reference signal. Each parameter set $\vec{x}$ has upper bounds set $\vec{u}$ and lower bounds set $\vec{l}$, which are point-wise compared in Eq (4). The optimization problem was solved using an implementation of PSO from MATLAB® Global Optimization Toolbox. The PSO options were, *MaxIterations* 5000, *MaxStallIterations* 50, and *FunctionTolerance* 10^{-5}. At the point of PSO termination, local minimization function *fmincon* was called from the MATLA ® Global Optimization Toolbox to identify the local minima. As PSO is a population-based global optimization framework, there is a degree of randomness in the final termination point, therefore we ran five PSO iterations for each individual recording, and the final fitted parameter values were those that resulted in the lowest RD amongst the five PSO iterations.

$$\min_{\vec{x}} RD(g(t, \vec{x}), \phi_r), \quad \vec{l} \le \vec{x} \le \vec{u} \tag{4}$$

$$RD(\phi_r, g(t, \vec{x})) = \frac{(\phi_r - g(t, \vec{x}))\cdot(\phi_r - g(t, \vec{x}))}{\phi_r \cdot \phi_r} \tag{5}$$

The bounds $\vec{l}$ and $\vec{u}$ used for the global optimization problem are summarized in Table 1. To model both the positive amplitudes of the R-wave and the often negative amplitudes of the Q, S waves, *amp* can vary between values of 1 and − 0.2 times the maximum potential found in the median ECG recording. As median ECG recordings from different

Table 1
Summary of model bounds for healthy subjects.

Parameter	*amp*	*width*	*shift*	b_s
upperbound (u)	$1 \times max\ pot.$	0.1	1	0.1
lowerbound (l)	$-0.2 \times max\ pot.$	0.001	0	−0.1

subjects may be different in length, in order to provide unified bounds for all recordings, the time parameter t for the Gaussian basis, as well as the bounds for parameters *width* and *shift* are expressed in *normalized heartbeat time*. The *normalized heartbeat time* is defined to be the sample number divided by the total number of samples in a median ECG recording, resulting in 0 and 1 being the start and end of the median ECG recording, respectively. The total number of samples in the median ECG recording is saved for scaling *normalized heartbeat time* into samples.

The bounds for *width* found in Table 1, limit any single Gaussian basis component to be between 0.001 and 0.1 of *normalized heartbeat time*, which is consistent with reference recordings from healthy subjects not having any single complex exceeding 25% of the *normalized heartbeat time*. The parameter shift have bounds between 0 and 1 in *normalized heartbeat time*, as peaks for ECG complexes may happen any time during the beat. Finally, b_s, intended to model isoelectric baseline shift, can vary between − 0.1 and 0.1, as the median recordings from the ECGRDVQ database are preprocessed with minimal isoelectric shift.

2.3. Identifying overlapping basis function groupings which represents the same P, Q, R, S or T-wave (Step 3)

Gaussian bases are generally viable for representing the individual P, Q, R, S, T-wave of an ECG. However, in an error minimizing global optimization framework, its symmetrical nature often forces multiple overlapping Gaussian functions to be summed to represent the same complex in cases where the individual waves are skewed or otherwise asymmetrical in morphology. Therefore, fitted Gaussians $w_j \subseteq w_i$ which significantly overlap to represent the same complex must be considered together as a grouping. In this paper, we consider any two or more basis functions to be overlapping if the *shift* of one basis function lies within two standard deviations, or $\frac{2width}{\sqrt{2}}$, of the *shift* of the other basis functions. Intuitively, each grouping can be thought of as a subset of fitted basis functions which represent a particular complex of the ECG morphology. Fig. 2 shows the identification of overlapping basis function groupings from fitted Gaussian basis functions.

2.4. Automated identification of J, T_{peak} and T_{end} (Step 4)

There exists many automated algorithms for delineation of ECG complexes [14,15]. The method proposed here aims to identify similar timing intervals compared to clinical experts. We focus on the J, T_{peak}, and T_{end} timings as the four drugs used in this work have been clinically noted to have different effects on repolarization. It is well known that the inflection points at the point of maximum descending gradient for the Gaussian basis function can be found one standard deviation from the mean. In the case of the ECG model basis functions found as in Eq (2), the maximum gradient for each basis component is dependent on the *amp* and *width* parameters and can be analytically solved as in Eq (6) (see Appendix B). With this gradient, each of the Gaussian basis can be approximated into a triangle and the individual triangle waves can be summed to form a whole ECG triangular approximation of the Gaussian basis fit.

$$maxgradient_i = \frac{e^{-0.5} \cdot \sqrt{2} \cdot amp_i}{width_i} \tag{6}$$

As ECG complexes are often asymmetric in shape, multiple overlapping basis functions may be fitted to represent the actual complex morphology. Therefore, the identification of the J, T_{peak} and T_{end} timings

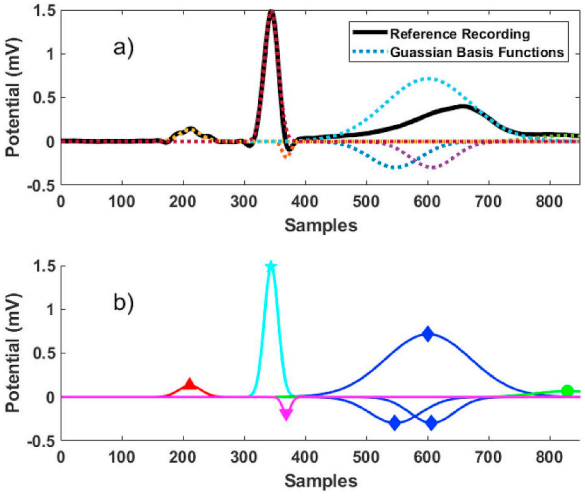

Fig. 2. An example of Gaussian basis function descriptions of ECG. a) A clinical ECG recording (black) decomposed into Gaussian basis functions (dotted) using methods described in Section 2.2. b) The individual functions in overlapping basis function groups. Peaks are identified by diamonds. There are 3 basis functions (blue) representing the T-wave. The group identification is described in Section 2.3.

must be considered in terms of overlapping basis function groupings. The peak of any overlapping basis function grouping is the point of *largest positive* deviation of basis function grouping from the baseline b_s. The start and end of any overlapping basis function grouping are the points at which the triangle approximation first and last deviate from the baseline b_s, respectively. The amplitude of the isoelectric line is identified automatically as the b_s parameter during the parameter identification step (Section 2.2). Identification of J from LII and Tpeak and Tend from lead VM uses similar criteria to expert annotation [3]:

1. The R-wave is defined to be the basis function grouping with the largest positive *amp*. This is found with the LII triangle approximation, and marked with a black star in Fig. 3.
2. The J point is defined to be the point of transition between the end of the QRS complex and the start of the ST segment. However, this transition is not sharply demarcated, and therefore the J point is difficult to measure, with discrepancies of up to 40 ms in repeated measurements [16,17]. The whole ECG LII triangle approximation to algorithmically search for a J point within 100 ms *after* the R peak.
   (a) If there is an overlapping basis function grouping which represents a trough and ends within a 100 ms window, as in Fig. 3a, take the end of this trough as the *search start point*.
   (b) If no such overlapping basis function grouping with a trough exists within this window, as in Fig. 3b, the *search start point* is the last point at which the gradient of the whole triangle wave is negative within this 100 ms window.

This *search start point* has been marked as the right pointing triangle in Fig. 3. Calculate the moving sum of the previous 3 samples for the absolute value of the triangle wave gradient from the *search start point* to the end of the 100 ms window, the minimum point of this moving sum is the J point.

3. For the fitted lead VM, any overlapping basis function grouping that has at least 0.8 times the largest positive amplitude of all basis function groupings with peak occurring *after* the J point is a T-wave candidate. The T-wave candidate, which peaks first is defined to be the T-wave. This definition detects the first peak of any notched T-wave as the T_{peak}. Fig. 3a identifies the notched T-wave timings, while Fig. 3b identifies timings for a normal T-wave.

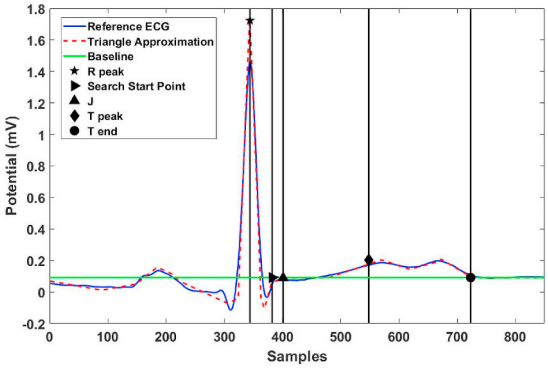

(a) With trough within 100ms of R peak.

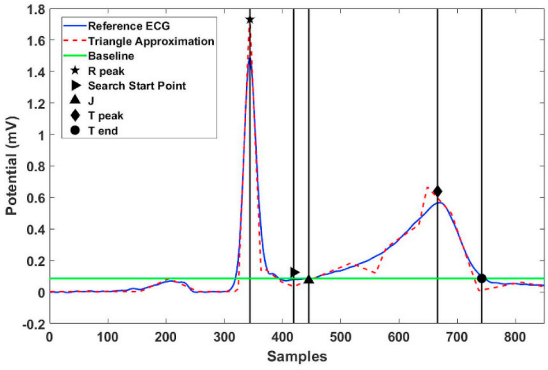

(b) No trough within 100ms of R peak.

Fig. 3. Approximated triangle wave of reference ECGs and the identified J, T_{peak}, *search start point* and T_{end} timings. The triangle wave is the linear combination of the triangle approximation of the individual fitted Gaussian basis functions. The vertical lines extending from the marked timings aid to identify the points on the clinically recorded reference median ECG wave. The isoelectric baseline (b_s) is marked by the green line.

4. For the fitted lead VM, from the last occurring overlapping basis function grouping T-wave candidate, identify the point at which the triangle approximation of this T-wave candidate crosses the isoelectric line (b_s), which has been marked as the green line in Fig. 3; this is the T_{end}.

2.5. Prediction of post-drug waveform morphology (Step 5)

A benefit of decomposing clinical ECG recordings to a parametric Gaussian basis function model is that the fitted parameters represent the clinical recording in a reduced parameter space of Gaussian waveforms. We leverage this to quantify signal morphology changes between the pre-drug and post-drug states. The parameter changes are applied to the fitted parameters from pre-drug recordings to predict corresponding post-drug parameters and signals. The data for all four drugs, as preprocessed from Section 2.1, were split into training and testing sets. We quantitatively assessed our proposed prediction strategy using a leave-one-out cross validation strategy. For each of the four drug states, in each cross validation iteration, pre-drug and post-drug ECGs from all-but-one subject serve as the training set, and the pre-drug and post-drug ECGs from the left-out subject serve as the testing set. The cross validation iterations stop when each subject has been in the testing set once. Fig. 4 provides an overall summary for *one* cross validation iteration of the proposed approach. The individual Gaussian functions shown in Fig. 4 are visual representations, in reality each Gaussian is characterized by and compared through *amp*, *width*, and *shift* parameters.

Observing the changes in fitted ECG model parameter values due to drug effects, Step 5a from Fig. 1 and the first dashed box of Fig. 4, can be described as follows.

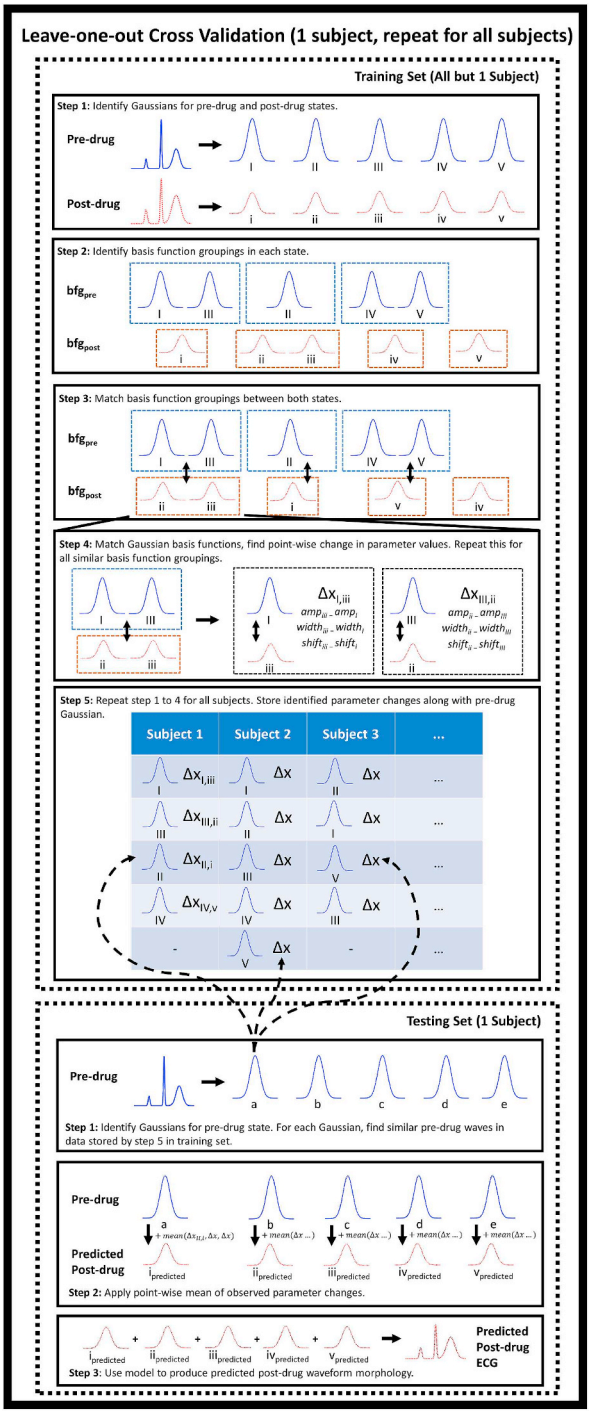

Fig. 4. Training and testing methodology for predicting post-drug waveform morphology.

1. Gather pre-drug and post-drug median ECG recordings from the same subject, and identify Gaussian basis function model parameter values using methods from Section 2.2. In Fig. 4, the fitted Gaussians have been labelled to be easily identified throughout the process, with I, II, III, IV, and V corresponding to the pre-drug fitted Gaussians, and i, ii, iii, iv, and v corresponding to the post-drug fitted Gaussians.
2. Use methods from Section 2.3 to identify the basis function

groupings for both pre-drug (bfg_{pre}) and post-drug (bfg_{post}) parameter sets, these have been separated using dotted boxes in Fig. 4. Also calculate the mean representative parameter values: R_{amp} and R_{shift}, for each basis function grouping, by taking the arithmetic mean of the *amp*, *width*, *shift* parameters in that grouping.

3. For each grouping in bfg_{pre}, identify the paired grouping in bfg_{post} with the smallest Euclidean distance, not exceeding a threshold of 0.2, using the arithmetic mean of *amp* and *shift* for both groupings. This threshold value is based on 10% of the maximum available change within the parameter bounds for *shift* and *amp*, as seen in Table 1; *width* was not used, as the length of waveforms, especially the T-wave, can vary greatly between pre-drug and post-drug states. Note in Fig. 4, some groupings with multiple Gaussians may be matched to that with single Gaussians (e.g. IV and V matched with v) and some groupings may not be within distance threshold of any other grouping (e.g. iv).
4. For each Gaussian from a given bfg_{pre} grouping, find the similar Gaussian in the paired bfg_{post} with the smallest Euclidean distance between parameter values not exceeding a distance threshold of 0.1418. This threshold was chosen as it is 10% of the total Euclidean distance between minimum and maximum bounds, not accounting for baseline shift b_s, for the parameter values found in Table 1. Calculate the differences in parameter values Δx of pre-drug *amp*, *width*, and *shift* values subtracted from post-drug values, between the similar basis function pairs.
5. Store the observed differences in parameter values Δx along with parameter values from the pre-drug basis function.

Applying the training set parameter changes to predict the post-drug ECG morphology, Step 5b from Fig. 1 and the second dashed box in Fig. 4, can be described as follows.

1. For the test subject, identify the Gaussian basis function for the pre-drug median recording using the methodology in Section 2.2. In Fig. 4 the identified Gaussians are labelled as *a*, *b*, *c*, *d*, and *e*. For each of the testing Gaussian basis functions, find all pre-drug training basis functions with parameters that are within the threshold 0.0709 Euclidian distance of the testing basis parameters. This threshold was chosen as it is 5% of the total Euclidean distance between minimum and maximum bounds, not accounting for baseline shift b_s. The corresponding parameter differences from the training set are *D*. In Fig. 4, three waves from the training set were found to be within threshold for Gaussian wave *a* (indicated by the dashed arrows), therefore, three Δx are a part of D_a. The similar waves for *b*, *c*, *d*, and *e* were not shown for clarity.
2. Find the arithmetic mean differences of *amp*, *width*, and *shift* values within *D* from the training set. Add the mean differences to the testing *amp*, *width*, and *shift* values to get predicted post drug parameter values for the testing Gaussian basis functions.
3. Calculate the predicted post-drug ECG waveform by using the parametric model with the predicted parameters.

3. Results

In this section, clinical data from the ECGRVDQ database [3,13], is used to show the efficacy of the proposed methodology.

3.1. Gaussian basis model representation of clinical ECGs

This subsection presents results after Step 2 from Fig. 1. To demonstrate the Gaussian basis parametric model, the LII median ECG from the post-drug record of subject number 1 from the Dofetilide dataset was parametrized using a varying number, *N*, of Gaussian basis functions (Eq (3)). Fig. 5 shows the mean value of the objective function and the mean PSO computational time across all five iterations of PSO fits as a function of *N*. As expected, the mean objective function value

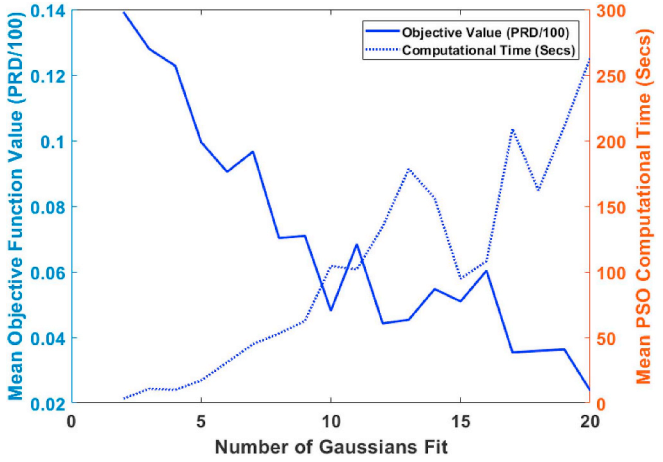

Fig. 5. The mean RD objective function value ($\frac{PRD}{100}$) in solid line, y-axis left; and the mean PSO computational time (seconds) in dotted line, y-axis right, as functions of the number of Gaussians fit. The plotted value is from the mean of the 5 different PSO fits conducted at each number of Gaussians fit.

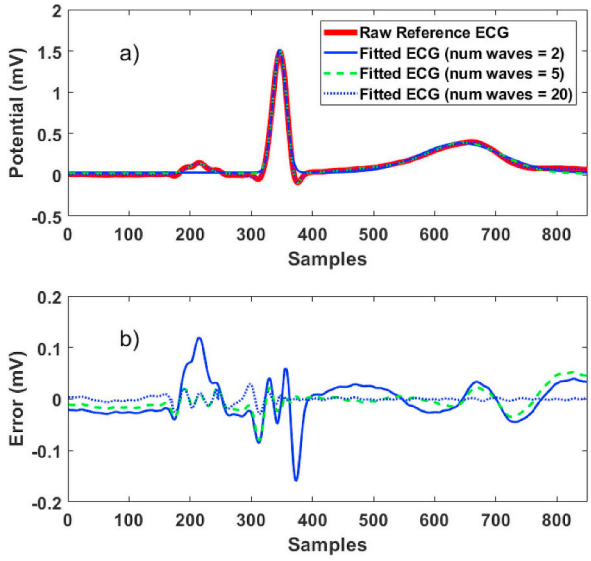

Fig. 6. Waveform and error comparisons. a) Clinical ECG (red) compared to Gaussian representations with varying numbers of waveforms *N*. b) The error between the clinical ECG and the Gaussian representations.

decreases and the mean computational time for PSO fit increases as *N* increases.

To help illustrate the temporal efficacy of the Gaussian basis to represent ECGs, Fig. 6 demonstrates the raw reference wave relative to a set of fitted representations at different *N*, and the error between the representation and clinical recording in the time-domain. At $N = 2$, only the R and T-wave are represented, at $N = 5$, the R, T, P, and S waves are represented, and at $N = 20$ characteristic P, Q, R, S, and T-waves of the normal sinus rhythm ECG are all represented. As *N* increases, the time-domain error also decreases, but this may also lead to over-fitting.

3.2. Identification of J, T_{peak} and T_{end} intervals

This subsection presents results after Step 4b in Fig. 1. Fig. 7 shows the proposed method of determining *J*, T_{peak}, and T_{end} on all pre-processed 22 recordings in the Dofetilide pre-drug state. All waves shown here were fitted using $N = 7$. Fig. 7 overlays the *J* timings found using the Lead II and the T-wave timings found using the vector

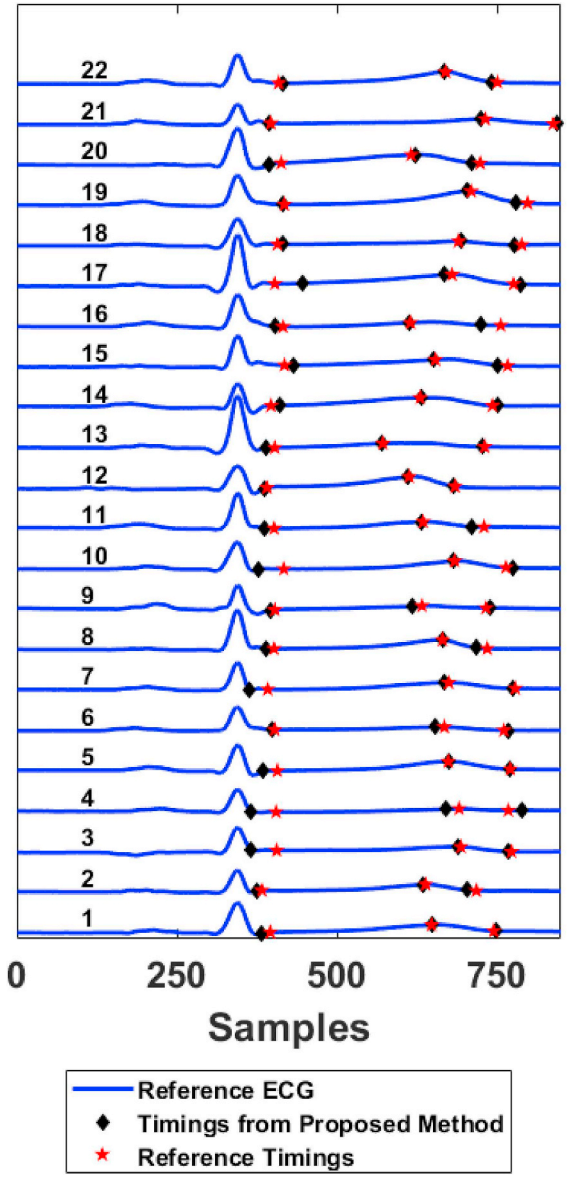

Fig. 7. The detected J, T_{peak}, and T_{end} times for all 22 recordings from the Dofetilide post-drug dataset using the fitted Gaussian model parameters (N = 7). The values calculated using the method from Section 2.4 are marked as the black diamonds. The ECG timing annotations from Ref. [3] are marked as the red stars. Note here that the J timing is found using LII, while T_{peak} and T_{end} are found using the VM lead.

magnitude lead on the Lead II reference ECG recordings.

We quantitatively assess the ability for the proposed method to capture the J to T_{peak} and T_{peak} to T_{end} ECG intervals. Fig. 8 are the swarm plots of the detected times for the two intervals in both the pre-drug and post-drug states for all 4 drug states. Table 2 and Table 3 shows the mean detected interval lengths and the standard deviations for both the proposed method and the expert annotated times. The paired sample t-test p-values from both tables suggest that we cannot reject the null hypothesis that the difference between intervals detected via expert annotated timings and proposed method have zero mean at a significance level of 0.05 ($p > 0.05$). The exception is the T_{peak} to T_{end} interval in the Dofetilide pre-drug state. Therefore, we conclude that the proposed method is able to assess the timing intervals correctly.

With $N = 7$, the mean change in T_{peak} to T_{end} intervals and J to T_{peak} intervals between pre-drug and post-drug states calculated from expert annotated intervals reported in Ref. [3] and those calculated using the proposed method in Section 2.4 can be found in Table 4 and Table 5, respectively. Paired-sample t-test p-values ($p > 0.05$) suggest that the mean change in T_{peak} to T_{end} and J to T_{peak} intervals between pre-drug and post-drug states detected by our method are *not* significantly different to expert annotated [3], for any of the four drugs. Note here that the J point is found with Lead II (LII), while the T_{peak} and T_{end} times are found using the vector magnitude lead (VM).

3.3. Prediction of post-drug ECG

This subsection presents results after Step 5b of Fig. 1. Predicted post-drug ECG were determined for varying numbers, N, of Gaussian basis functions. Fig. 9 shows the Pearson correlation coefficient (PCC) values between the predicted post-drug waveform and the clinically recorded post-drug waveform for individual subjects across all N. Note here that at $N = 20$, the mean PCC decreases from that found in lower N for all four drug cases, suggesting larger N leads to over-fitting. In this section, we show fits of $N = 7$ throughout the prediction process for all four drug states, as the average PCC across all prediction cases (black circles and black triangles in Fig. 9) is close to maximum levels for all 4 drug states while having minimal chance of over-fitting.

Fig. 10 shows the changes in T-wave model parameters from the vector magnitude lead. Fig. 10a and b show that for Dofetilide and Quinidine, the T-wave is almost always longer (increase in *width*) in the post-drug case. However, increases in T-wave length (*width*) are not found in Fig. 10c or 10d for Ranolazine and Verapamil, respectively.

Fig. 11 and Fig. 12 show the time-domain representation of predicted LII and VM lead post-drug ECG waveforms for $N = 7$ compared to the clinically recorded post-drug ECG, respectively. The time-domain morphologies were calculated from pre-drug fitted Gaussian basis model parameters using the framework outlined in Section 2.5. The mean PCC between predicted and recorded full waveform morphologies can be found in Table 6. Note here that the mean PCCs are all above 0.9, and approaching the ideal value of 1. The mean PCC for all predictions across all drug states and both VM and LII is 0.94 ± 0.05. The recorded and predicted post-drug ECG are significantly correlated for all prediction cases ($p < 0.01$) using PCC.

4. Discussion

We have shown that modeling clinical ECG signals using Gaussian basis sets and a global optimization framework [9] effectively captures temporal and morphological features of the signals. Here we have comprehensively tested and analyzed the approach.

The Gaussian bases are not orthonormal. However, we have shown that an increasing number of basis functions decreases the error between model and recorded morphology [10]. With an increasing number of basis functions the computational cost increases. Fig. 5 shows that the mean computational time for each PSO run is between 5 and 200 seconds. With algorithm refinement and parallelization [18] this will be significantly improved. Our current procedure using five PSO fits followed by a local gradient descent has proved effective. However, ongoing work includes deeper investigation of how fitted Gaussian model parameters vary with scaling and bounds, objective function scaling and selection and the PSO algorithm parameters.

Other basis models, such as Fourier functions, have been used to accurately reconstruct ECG using a larger number of basis functions that we have required with Gaussian bases [10]. The non-compact nature of Fourier bases means they cannot be directly linked to particular ECG complexes. Previous work has segmented the ECG first into multiple complexes and then modeled each complex with Fourier harmonics [19]. In this paper we have shown that the Gaussian bases approach naturally segments the ECG complexes during the parameter identification process.

The Gaussian basis function (Eq. (2)) is symmetric and cannot directly represent the asymmetric complexes often found in ECG

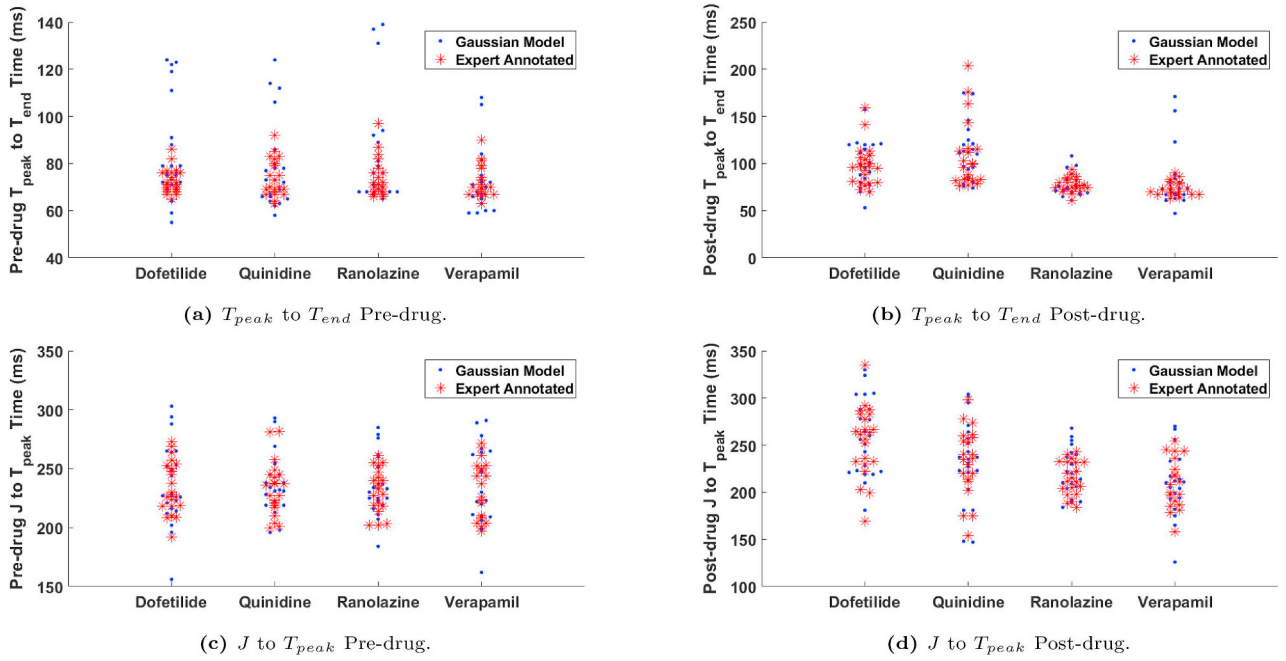

(a) T_{peak} to T_{end} Pre-drug.

(b) T_{peak} to T_{end} Post-drug.

(c) J to T_{peak} Pre-drug.

(d) J to T_{peak} Post-drug.

Fig. 8. Swarm plot of the timing intervals detected using the proposed method (dots) and the expert annotated timing intervals (astrisks).

Table 2
Summary of detected T_{peak} to T_{end} intervals.

Drug State	Dofetilide	Quinidine	Ranolazine	Verapamil
Expert Pre-drug [3]	72.5 ± 5.12*ms*	73.8 ± 7.89*ms*	74.0 ± 8.14*ms*	72.2 ± 6.87*ms*
Our Pre-drug	84.0 ± 21.5*ms*	78.7 ± 19.0*ms*	83.8 ± 24.0*ms*	75.3 ± 19.7*ms*
Paired Sample T-test p-value Pre-drug	0.0219	0.2218	0.0878	0.1910
Expert Post-drug [3]	97.6 ± 21.4*ms*	108.2 ± 35.4*ms*	77.4 ± 7.86*ms*	73.5 ± 7.70*ms*
Our Post-drug	98.0 ± 24.2*ms*	110.5 ± 29.3*ms*	77.5 ± 12.1*ms*	83.0 ± 32.3*ms*
Paired Sample T-test p-value Post-drug	0.9130	0.6450	0.9857	0.1910

Table 3
Summary of detected J to T_{peak} intervals.

Drug State	Dofetilide	Quinidine	Ranolazine	Verapamil
Expert Pre-drug [3]	234.5 ± 22.0*ms*	233.3 ± 22.7*ms*	231.8 ± 18.3*ms*	232.8 ± 24.2*ms*
Our Pre-drug	237.5 ± 34.6*ms*	237.5 ± 25.0*ms*	235.8 ± 25.9*ms*	232.7 ± 32.9*ms*
Paired Sample T-test p-value Pre-drug	0.6119	0.3171	0.3865	0.9763
Expert Post-drug [3]	254.5 ± 36.9*ms*	232.8 ± 36.1*ms*	215.0 ± 18.3*ms*	209.3 ± 26.9*ms*
Our Post-drug	258.9 ± 40.8*ms*	232.5 ± 43.8*ms*	217.9 ± 24.1*ms*	208.8 ± 34.9*ms*
Paired Sample T-test p-value Post-drug	0.3309	0.9618	0.5975	0.9471

Table 4
Summary of detected change in T_{peak} to T_{end} intervals.

Drug State	Dofetilide	Quinidine	Ranolazine	Verapamil
Expert [3]	25.0 ± 19.6*ms*	34.4 ± 31.2*ms*	3.4 ± 6.26*ms*	1.26 ± 5.46*ms*
Proposed	14.0 ± 36.4*ms*	31.8 ± 32.8*ms*	− 6.30 ± 23.9*ms*	7.68 ± 32.1*ms*
T-test p-value	0.0945	0.6433	0.0705	0.4026

recordings. Fig. 2 demonstrates that our method represents asymmetrical complexes by fitting overlapping basis functions to create a group of bases for that complex. This is an advantage of the global optimization method of Section 2.2 and improves on the one-wave-per-complex local optimization with pre-processed initial parameter points [20]. Alternative approaches have used Gaussian mesa functions for ECG modeling [11] and analysis of repolarization morphology [12]. These are piecewise continuous functions with an initial and end Gaussian segment and a flat mesa between them. This enables asymmetric and flattened complexes to be modeled without using overlapping basis function groups. In some instances a basis with a flat top may not be the most appropriate and future investigation of alternative piecewise functions with more flexibility will be made.

An important finding in this work is that the mean J to T_{peak} and T_{peak} to T_{end} intervals calculated by our Gaussian decomposition of the ECG are statistically similar to expert annotations [3] in both control and drug states. The triangle based method we have used is a robust approach for determining timing measure, including identifying the J point. This is beneficial for objectively identifying these measures over large databases of many ECG signals. A caveat is that while we found that $N = 7$ Gaussians basis functions have been adequate to represent all the complexes in the signals we have tested, too few will underrepresent the signal and affect determination of timing measures.

The pre- and post-drug changes in parameter values in Fig. 10 show that they encode ECG morphology changes due to drug effects. It

Table 5
Summary of detected change in J to T_{peak} intervals.

Drug State	Dofetilide	Quinidine	Ranolazine	Verapamil
Expert [3]	$20.0 \pm 24.4ms$	$-0.57 \pm 28.2ms$	$-16.8 \pm 14.4ms$	$-23.6 \pm 14.9ms$
Proposed	$21.4 \pm 37.6ms$	$-5.05 \pm 39.6ms$	$-17.9 \pm 30.2ms$	$-23.8 \pm 31.5ms$
T-test p-value	0.8096	0.4201	0.8577	0.9688

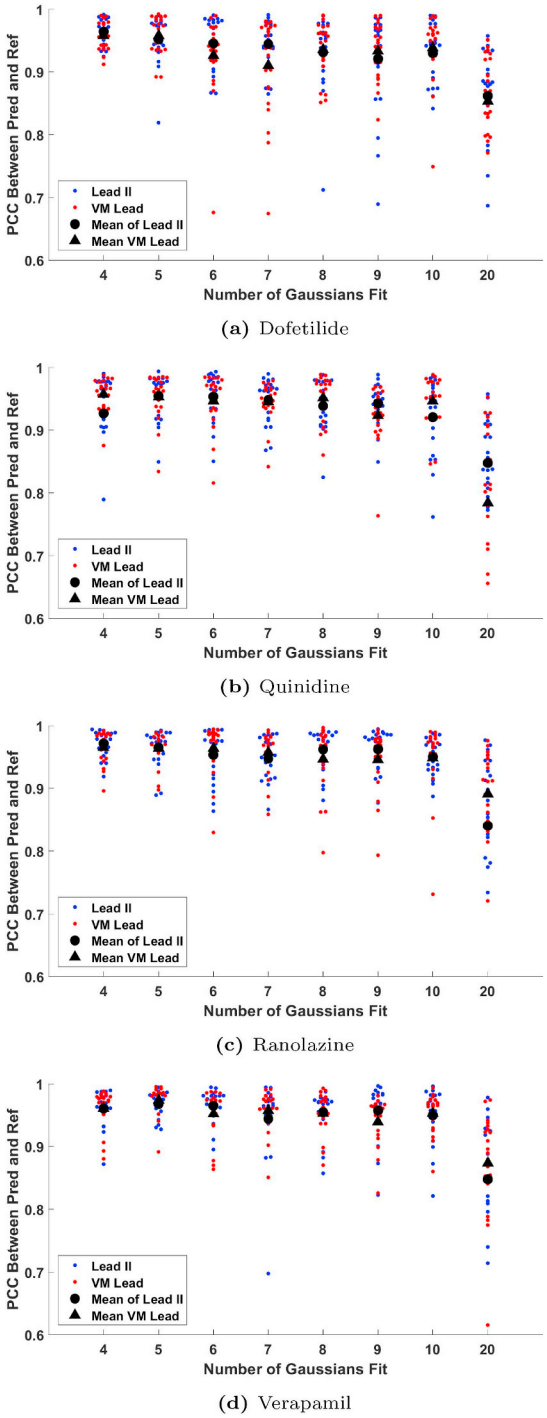

Fig. 9. The PCC between the predicted and the clinically recorded post-drug ECG for both Lead II (LII) and vector magnitude lead (VM) as a function of number of Gaussians fit (N). The training set used during the prediction of each individual ECG recording is composed of all other recordings of the same lead under the same drug effect (leave-one-out cross validation). PCC for individual recordings are marked in colored dots, Lead II (blue) and VM lead (red). The mean PCC of all recordings at each N is the marked as black circle (Lead II) and black triangle (VM lead).

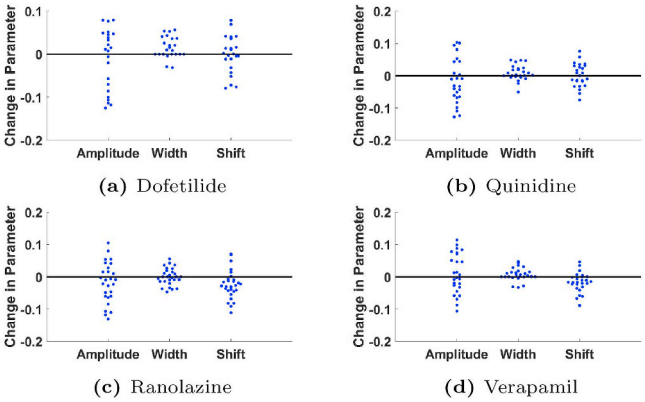

Fig. 10. The changes in T-wave parameter values detected in the training set from the vector magnitude lead. Vector magnitude lead is used to calculate the T_{peak} and T_{end} times. The parameter changes here are detected using $N = 7$. The black solid line indicates the point of zero parameter change.

demonstrates that in general there is an increase in T-wave length (*width*) from pre-to post-drug states for both Dofetilide and Quinidine and little change for Ranolozine and Verapamil. These observations are physiologically sound as Dofetilide and Quinidine block the hERG potassium channels which results in prolonged repolarization times and longer T-waves [3]. Ranolazine and Verapamil facilitate late sodium current block and strong calcium block, respectively. This opposes hERG channel effects on early repolarization and causes little to no change in the Tpeak and Tend interval [3].

Good predictions of post-drug ECG waveform morphology is found by applying observed changes in the Gaussian basis function parameter space (Section 2.5) using a leave-one-out cross validation strategy. The prediction method applies observed changes in parameter values from the training set to fitted parameters from a never-seen-before pre-drug ECG in the testing set. This efficacy of this strategy is demonstrated using both the VM and the LII leads. The mean PCC for all waveform predictions across VM and LII for all four drug states was very high at 0.94 ± 0.05 and shows that in general the ECG morphologies of the post-drug state were well predicted. The number of Gaussian basis functions used for prediction in all four drug cases was $N = 7$. When N is large the complexes are overfit and there are redundant basis functions [10], each of which has to be accounted for when applying parameter shifts. Overfit complexes are unsuitable for predicting waveform morphologies. Prediction of whole ECG morphology corresponds with the comprehensive waveform analysis explored in Ref. [21], from which the CiPA suggested J to Tpeak timing interval is derived. The comprehensive analysis includes T-wave biomarkers such as notching, asymmetry, and flatness that can only be captured through morphology and not timing intervals alone [21]. This is further supported for post-drug ECG signal morphology analysis.

The Gaussian basis approach to predicting drug effects on a patient's ECG, relies on there being similar ECG examples in the training dataset. The range of conditions, e.g. patho-physiological state, gender, drug-combinations, etc., in the training data must be carefully considered prior to using the Gaussian basis parameter space for prediction. This is particularly the case for Dofetilide and Quinidine, for example, as there are potential distortions in the T-wave, such as inverted, notched,

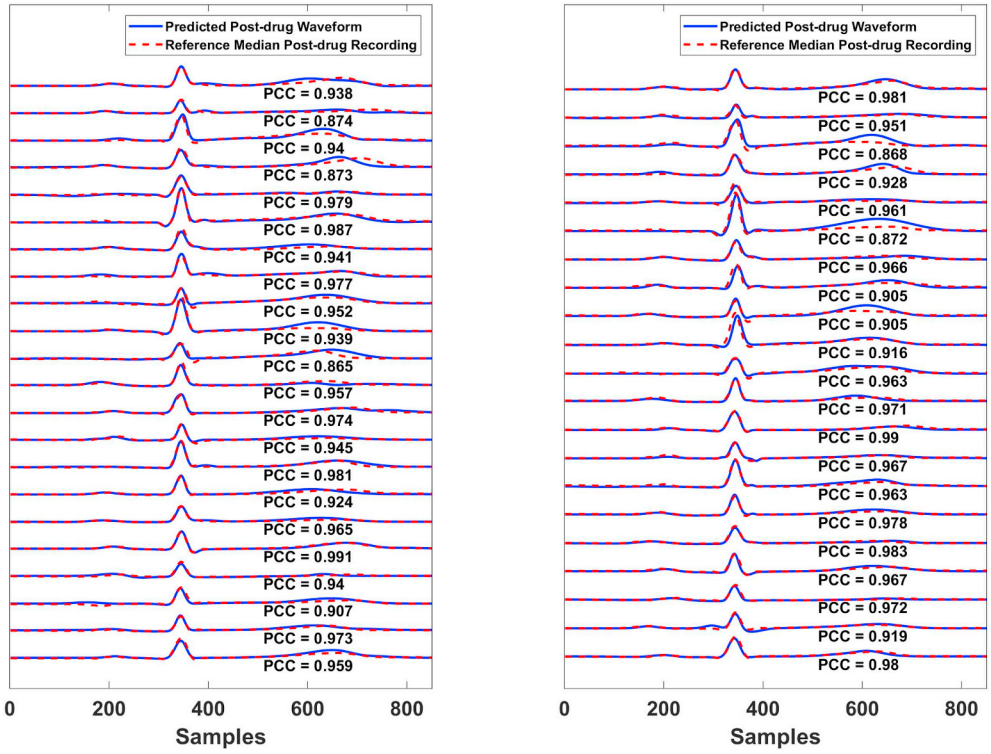

(a) Dofetilide

(b) Quinidine

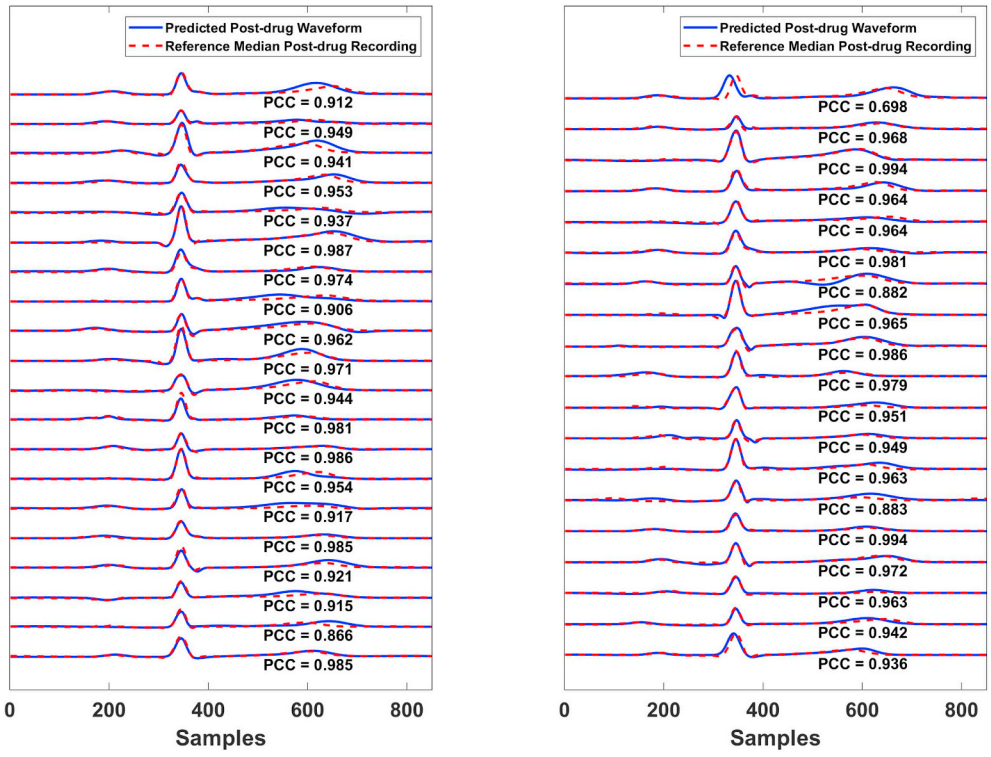

(c) Ranolazine

(d) Verapamil

Fig. 11. Time-domain representation of predicted full post-drug waveform morphology at $N = 7$ (blue solid line) and the clinical median post-drug recording (red dotted line) for Lead II. The PCC between the two time-series is also shown. The PCC associated p-values are <0.01 for all predictions, suggesting that the PCC are statistically significant.

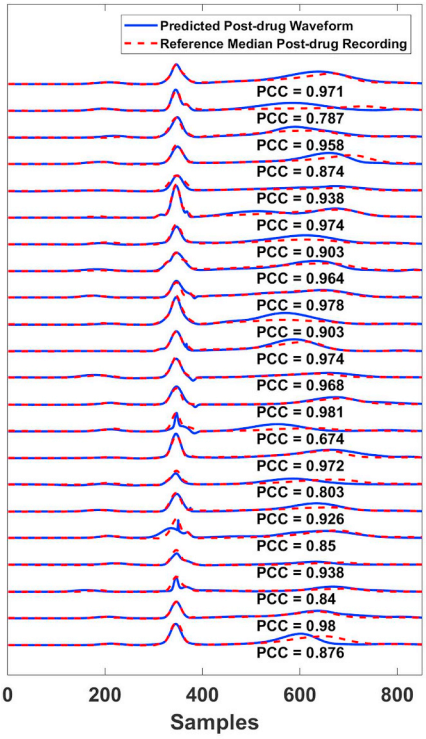

(a) Dofetilide

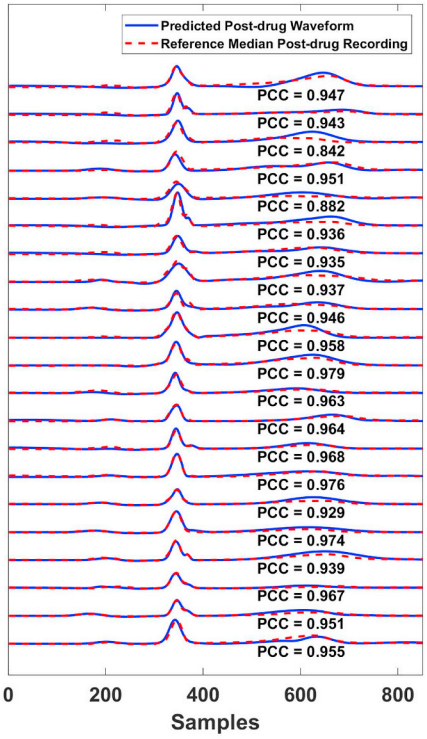

(b) Quinidine

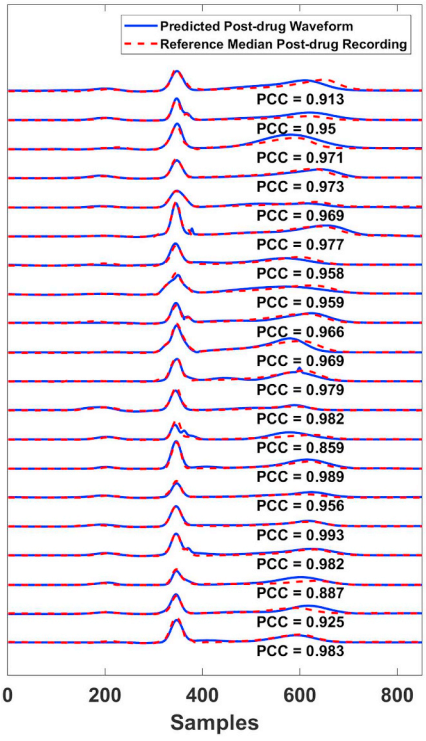

(c) Ranolazine

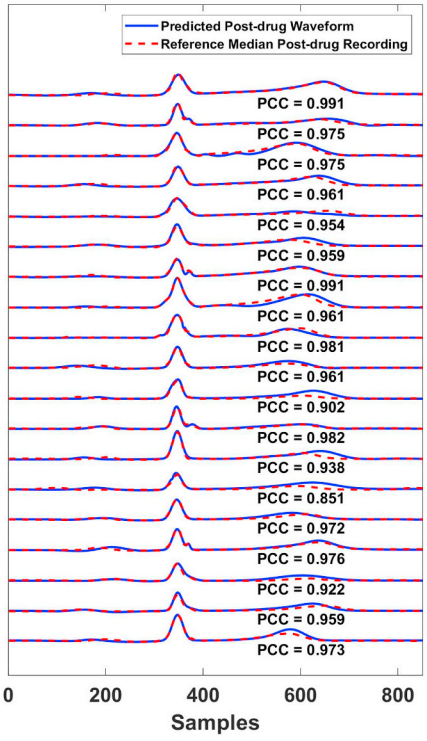

(d) Verapamil

Fig. 12. Time-domain representation of predicted full post-drug waveform morphology at $N = 7$ (blue solid line) and the clinical median post-drug recording (red dotted line) for vector magnitude lead. The PCC between the two time-series is also shown. The PCC associated p-values are <0.01 for all predictions, suggesting that the PCC are statistically significant.

Table 6
Summary of PCC between predicted and clinically recorded ECGs for lead II (LII) and vector magnitude lead (VM) ($N = 7$).

Drug State	Dofetilide	Quinidine	Ranolazine	Verapamil
LII PCC	0.9444 ± 0.0368	0.9479 ± 0.0367	0.9472 ± 0.0333	0.9438 ± 0.0671
VM PCC	0.9105 ± 0.0798	0.9449 ± 0.0318	0.9570 ± 0.0352	0.9570 ± 0.0342

biphasic or flattened waves, and these are often highly interesting and important features. The extracted dataset used in this work (Section 2.1) does not contain many examples of these features in the post-drug state. Future work will broaden the number of datasets with pronounced distortions in the T-wave to ensure more examples of these features in the training data.

The J to T_{peak} intervals have been considered in more detail in the Supplementary Material. Comparisons in these measures pre- and post-drug, and with expert annotations, are given and there is good correspondence at the individual data point level. The statistical population comparison was shown in Table 5. We note that uncertainty in expert annotations has previously been estimated at 40 ms [16,17] and our J time point can be up to 50 ms in error in the worst case scenario. These uncertainties have been accounted for in the Supplementary Material. We also note that the standard deviation in the expert annotated pre-to post-drug intervals are large (Tables 4 and 5). In the Supplementary Material Fig S8 we show that our prediction technique predicts changes in individual data point J to T_{peak} intervals within the 95% confidence interval from the expert annotated data. This arises because our prediction technique has captured the population trend in the timing intervals (see Table 5).

The prediction of ECG morphology using Gaussian basis function parameters is a potentially powerful tool for assisting drug administration decisions, enabling phenomenological descriptions of post-drug signals based on pre-drug ECGs. The Gaussian basis function model is an effective dimensional reduction tool for complex ECG signals. While the post-drug ECG prediction strategy presented in this paper is effective, as more signals become available for training alternative machine-learning based prediction strategies may become useful to understand the increasing complexity. Furthermore, in future work the ECG parameterization methods can be extended for classification of different ECG complexes [22], compression or filtering of signals [23], the prediction of safe or unsafe post-drug Gaussian parameter states, and prediction of ECG morphologies in the context of multiple concurrent drugs.

5. Conclusion

Parametric ECG model with Gaussian basis functions is an approach for studying drug effects on ECG waveform morphology. We took a bound constrained global optimization approach for model parameter identification. We showed that model parameter values could be used to calculate clinically useful information such as change in J to T_{peak} and T_{peak} to T_{end} intervals, similar to those found under the computer aided attention of an expert (paired-sample t-test $p > 0.05$). Furthermore, model parameters can characterize changes in ECG morphology due to drug effects and predict post-drug ECG morphologies from pre-drug states (Pearson correlation $p < 0.01$ for all cases). Models of changes in Gaussian parameter values for single drugs could potentially be combined to form ECG morphology predictions of multiple drug states. Our work provides an objective measure of ECG morphological information for future clinical studies and can be extended towards characterization and prediction of diseased cardiac states.

Authors' Contributions

T.P.: designed and carried out the study, analysis and interpretation and data, drafting and revising of the article, and final approval of the version to be submitted; M.L.T.: provided insight on study design, data analysis and interpretation, revising of the article critically for important intellectual content, and final approval of the version to be submitted; A. M.: provided insight on study design, data analysis and interpretation, revising of the article critically for important intellectual content, and final approval of the version to be submitted.

Conflict of Interest

All authors have no conflict of interest to report.

Acknowledgements

This work was funded by the National Science Challenges, Science for Technological Innovation, NZ, grant 3713917. M. L. Trew was supported by a grant from the Fondation Leducq.

Appendix A. Spread of Fitted Parameter Values

The meta-heuristic population-based optimization strategy of Particle Swarm Optimization (PSO) does not guarantee a global optimum. In our method we repeat PSO from different starting points five times for each ECG and then do a local gradient minimization search. The solution with the lowest objective function over these five samples is the final parameter set. Fig A1 shows the scatter in final parameter and objective function value when the number of PSO iterations is varied from 1 to 50 in one subject from the post-drug Dofetilide dataset. Five Gaussian basis functions were used in all cases. The objective function values (*fval*) and the isoelectric line (b_s) show very little variation over 1 to 50 PSO iterations. Gaussian basis functions 1–3 correspond to the R, T and P complexes respectively and show minimal parameter variation. The Gaussian basis functions 4 and 5 are grouped with the other basis functions to capture low amplitude asymmetries in the complexes and, hence, the objective function is less sensitive to their variation.

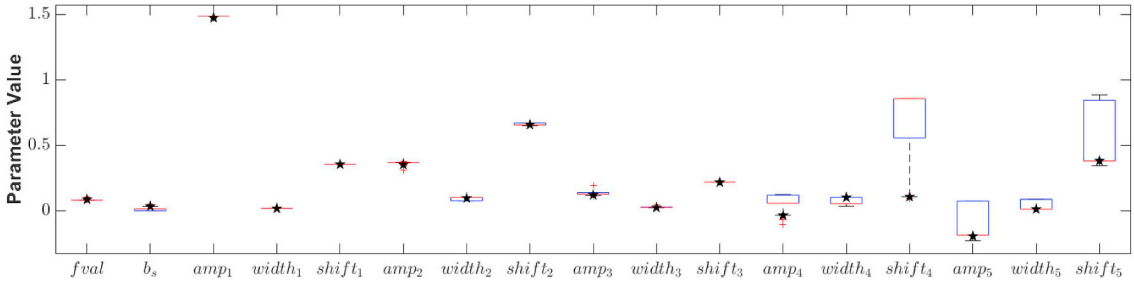

Figure A.1. The box-and-whisker plot of best objective function values (*fval*) and model parameters values from the iteration with the best *fval* for all number of PSO iterations (n_{pso} from 1 to 50). The black star marks the parameter values from 5 PSO iterations ($n_{pso} = 5$). The parameters were fitted to the post-drug recording of

subject number 1 from the Dofetilide dataset. The Gaussian model parameters here were sorted by *amp* after they have been identified.

Appendix B. Point of Maximum Gradient

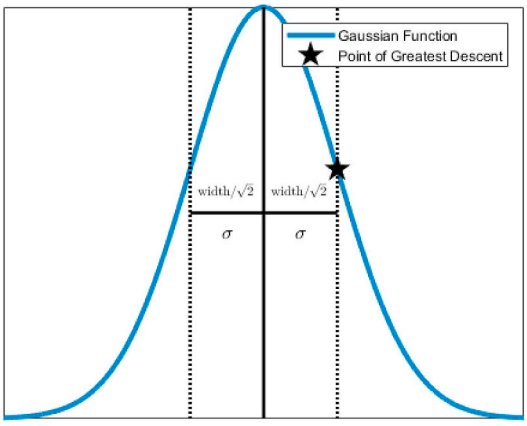

Figure B.1. Representation of point of greatest descent for a Gaussian function.

The parameter width in Eq (2) is related to the standard deviation σ of the standard Gaussian probability density function as shown in Eq (B.1). It is well known that the inflection point corresponding to the maximum descending gradient of the Gaussian probability density function is one standard deviation from the mean. The derivative of Eq (2) with respect to t regardless of *shift*, as it simply changes the position of the peak of the function, is shown in Eq (B.2). Substituting Eq (B.1) as t in Eq (B.2) gives Eq (B.3), which simplifies to Eq (6). Fig B1 demonstrates this point of greatest gradient descent on a Gaussian function.

$$\sigma_i = \pm\frac{width_i}{\sqrt{2}} \tag{B.1}$$

$$\dot{w_i}(t) = \frac{-2\cdot amp_i\cdot t\cdot\exp-\left(\frac{t}{width_i}\right)^2}{width_i^2} \tag{B.2}$$

$$\dot{w_i}(\sigma_i) = \pm\frac{-2\cdot amp_i\cdot\frac{width_i}{\sqrt{2}}\cdot\exp-\left(\frac{\frac{width_i}{\sqrt{2}}}{width_i}\right)^2}{width_i^2} \tag{B.3}$$

Appendix C. Predicted J to T_{peak} and T_{peak} to T_{end} Intervals

Fig C1 shows the difference between detected (Section 2.2) and predicted (Section 2.5) timing intervals compared to expert annotations [3] for all post-drug stages. Tables C1 and C2 show the means and standard deviations for the comparative data. The paired sample t-test p-values indicate that the detected and predicted intervals are similar to the expert annotations ($p > 0.05$). The exception to this is the T_{peak} to T_{end} interval in the Dofetilide post-drug stage.

Table C.1
Summary of Difference in T_{peak} to T_{end} Intervals Compared to Expert Annotations from Ref. [3].

Drug State	Dofetilide	Quinidine	Ranolazine	Verapamil
Detected	0.41 ± 17.3*ms*	2.29 ± 22.4*ms*	0.050 ± 12.3*ms*	9.53 ± 30.6*ms*
Predicted	16.5 ± 26.7*ms*	− 12.1 ± 41.8*ms*	14.5 ± 36.0*ms*	12.0 ± 21.7*ms*
T-test p-value	0.0445	0.1178	0.0713	0.7652

Table C.2
Summary of Detected Change in J to T_{peak} Intervals

Drug State	Dofetilide	Quinidine	Ranolazine	Verapamil
Expert [3]	4.32 ± 20.4*ms*	− 0.29 ± 27.0*ms*	7.25 ± 19.2*ms*	− 0.42 ± 27.3*ms*
Proposed	− 18.1 ± 53.8*ms*	3.24 ± 41.0*ms*	− 8.50 ± 40.2*ms*	− 3.84 ± 34.2*ms*
T-test p-value	0.0533	0.7370	0.505	0.7085

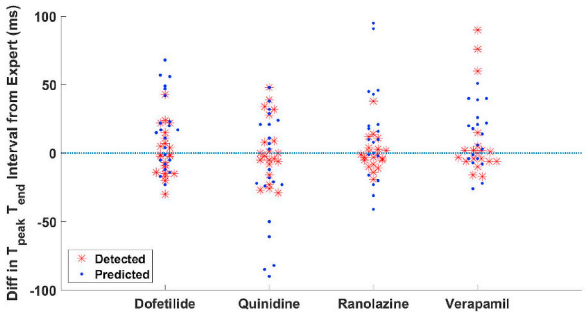

(a) Difference in T_{peak} to T_{end} Intervals to Expert Annotations.

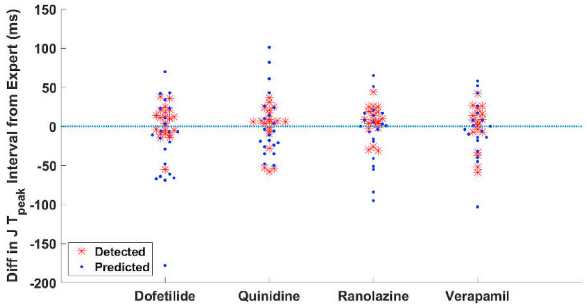

Figure C.1. Swarm plot of the difference in timing intervals compared to expert annotations [3]. Differences calculated using the intervals detected from fitted gaussian parameters ($N = 7$) from clinically recorded ECGs after Section 2.2 are marked as red astrisks; differences calculated from intervals detected after waveform morphology prediction after section 2.5 are marked as blue dots. The cyan dotted line indicates the line of zero difference in interval timing when compared to expert timings.

Supplementary data

Supplementary data to this article can be found online at https://doi.org/10.1016/j.compbiomed.2019.03.027.

References

[1] T. Colatsky, B. Fermini, G. Gintant, J.B. Pierson, P. Sager, Y. Sekino, D.G. Strauss, N. Stockbridge, The comprehensive in vitro Proarrhythmia Assay (CiPA) initiative update on progress, J. Pharmacol. Toxicol. Methods 81 (2016) 15–20, https://doi.org/10.1016/j.vascn.2016.06.002.

[2] L. Johannesen, J. Vicente, J. Mason, C. Erato, C. Sanabria, K. Waite-Labott, M. Hong, J. Lin, P. Guo, A. Mutlib, J. Wang, W. Crumb, K. Blinova, D. Chan, J. Stohlman, J. Florian, M. Ugander, N. Stockbridge, D. Strauss, Late sodium current block for drug-induced long QT syndrome: results from a prospective clinical trial, Clin. Pharm. Ther. 99 (2) (2016) 214–223, https://doi.org/10.1002/cpt.205.

[3] L. Johannesen, J. Vicente, J.W. Mason, C. Sanabria, K. Waite-Labott, M. Hong, P. Guo, J. Lin, J.S. Sørensen, L. Galeotti, J. Florian, M. Ugander, N. Stockbridge, D.G. Strauss, Differentiating drug-induced multichannel block on the electrocardiogram: randomized study of dofetilide, quinidine, ranolazine, and verapamil, Clin. Pharm. Ther. 96 (5) (2014) 549–558, https://doi.org/10.1038/clpt.2014.155.

[4] T.Y. Young, W.H. Huggins, On the representation of electrocardiograms, IEEE Trans. Biomed. Eng. 10 (1963) 86–95, https://doi.org/10.1109/TBMEL.1963.4322805.

[5] C. Caroubalos, C. Perche, C. Metaxaki-Kossinide, E. Sangriotis, D. Maroulis, Method for automatic analysis of the ECG, J. Biomed. Eng. 10 (4) (1987) 343–347.

[6] P.E. McSharry, G.D. Clifford, L. Tarassenko, L.A. Smith, A dynamical model for generating synthetic electrocardiogram signals, IEEE Trans. Biomed. Eng. 50 (3) (2003) 289–294, https://doi.org/10.1109/TBME.2003.808805.

[7] M. Rakshit, D. Panigrahy, P.K. Sahu, EKF with PSO technique for delineation of P and T wave in electrocardiogram(ECG) signal, 2nd International Conference on Signal Processing and Integrated Networks, SPIN 2015, 2015, pp. 696–701, , https://doi.org/10.1109/SPIN.2015.7095293.

[8] M.H. Vafaie, M. Ataei, H.R. Koofigar, Heart diseases prediction based on ECG signals' classification using a genetic-fuzzy system and dynamical model of ECG signals, Biomed. Signal Process. Control 14 (2014) 291–296, https://doi.org/10.1016/j.bspc.2014.08.010.

[9] T. Peng, M. Trew, A. Malik, Parametric modeling of electrocardiograms using particle swarm optimization, 2018 40th Annual International Conference of the IEEE Engineering in Medicine and Biology Society, EMBC, 2018.

[10] E.K. Roonizi, R. Sameni, Morphological modeling of cardiac signals based on signal decomposition, Comput. Biol. Med. 43 (10) (2013) 1453–1461, https://doi.org/10.1016/j.compbiomed.2013.06.017.

[11] R. Dubois, B. Quenet, Y. Faisandier, G. Dreyfus, Building meaningful representations for nonlinear modeling of 1d- and 2d-signals: applications to biomedical signals, Neurocomputing 69 (2006) 2180–2192.

[12] F. Badilini, M. Vaglio, R. Dubois, P. Roussel, N. Sarapa, I. Denjoy, F. Extramiana, P. Maison-Blanche, Automatic analysis of cardiac repolarization morphology using Gaussian mesa function modeling, J. Electrocardiol. 41 (6) (2008) 588–594, https://doi.org/10.1016/j.jelectrocard.2008.07.020 https://doi.org/10.1016/j.jelectrocard.2008.07.020.

[13] A.L. Goldberger, L.A.N. Amaral, L. Glass, J.M. Hausdorff, P.C. Ivanov, R.G. Mark, J.E. Mietus, G.B. Moody, C.-k. Peng, H.E. Stanley, PhysioBank, PhysioToolkit, and PhysioNet Components of a New Research Resource for Complex Physiologic Signals, (2000).

[14] M.E. Nygards, L. Sornmo, Delineation of the QRS Complex using the envelope of the ecg, Med. Biol. Eng. Comput. 21 (5) (1983) 538–547, https://doi.org/10.1176/ajp.152.8.1185.

[15] V.S. Chouhan, S.S. Mehta, N.S. Lingayat, Delineation of QRS-complex , P and T-wave in 12-lead ECG, J. Comput. Sci. Netw. Secur. 8 (4) (2008) 185–190.

[16] B. Surawicz, P. Macfarlanek, Inappropriate and confusing electrocardiographic terms J-wave syndromes and early repolarization, J. Am. Coll. Cardiol. 57 (15) (2011).

[17] B. Surawicz, E. Lepeschkin, The measurement of the duration of the QRS interval, Am. Heart J. 44 (1) (1952) 80–88.

[18] J.F. Schutte, J.A. Reinbolt, B.J. Fregly, R.T. Haftka, A.D. George, Parallel global optimization with the particle swarm algorithm, Int. J. Numer. Methods Eng. 61 (13) (2004) 2296–2315, https://doi.org/10.1021/nl061786n.Core-Shell arXiv:NIHMS150003.

[19] P. Kundu, R. Gupta, Electrocardiogram synthesis using Gaussian and fourier models, Proceedings of 2015 IEEE International Conference on Research in Computational Intelligence and Communication Networks, ICRCICN 2015, 2016, pp. 312–317, , https://doi.org/10.1109/ICRCICN.2015.7434256 December.

[20] G.D. Clifford, A. Shoeb, P.E. McSharry, B.A. Janz, Model-based filtering, compression and classification of the ECG, Int. J. Bioelectromagnetism 7 (1) (2005) 158–161.

[21] J. Vicente, L. Johannesen, J.W. Mason, W.J. Crumb, E. Pueyo, N. Stockbridge, D.G. Strauss, Comprehensive T wave morphology assessment in a randomized clinical study of dofetilide, quinidine, ranolazine, and verapamil, J. Am. Heart Assoc. 4 (4) (2015), https://doi.org/10.1161/JAHA.114.001615.

[22] P. Ravier, F. Leclerc, C. Dumez-viou, Redefining performance evaulation tools for real-time QRS complex classification systems, IEEE Trans. Biomed. Eng. 54 (9) (2007) 1706–1710.

[23] O. Sayadi, M.B. Shamsollahi, ECG denoising and compression using a modified extended Kalman filter structure, IEEE Trans. Biomed. Eng. 55 (9) (2008) 2240–2248, https://doi.org/10.1109/TBME.2008.921150.